Why Is CO$_2$ So Soluble in Imidazolium-Based Ionic Liquids?

Cesar Cadena, Jennifer L. Anthony, Jindal K. Shah, Timothy I. Morrow,
Joan F. Brennecke, and Edward J. Maginn*

*Contribution from the Department of Chemical and Biomolecular Engineering,
University of Notre Dame, Notre Dame, Indiana 46556*

Received November 15, 2003; E-mail: ed@nd.edu

Abstract: Experimental and molecular modeling studies are conducted to investigate the underlying mechanisms for the high solubility of CO$_2$ in imidazolium-based ionic liquids. CO$_2$ absorption isotherms at 10, 25, and 50 °C are reported for six different ionic liquids formed by pairing three different anions with two cations that differ only in the nature of the "acidic" site at the 2-position on the imidazolium ring. Molecular dynamics simulations of these two cations paired with hexafluorophosphate in the pure state and mixed with CO$_2$ are also described. Both the experimental and the simulation results indicate that the anion has the greatest impact on the solubility of CO$_2$. Experimentally, it is found that the bis(trifluoromethylsulfonyl)-imide anion has the greatest affinity for CO$_2$, while there is little difference in CO$_2$ solubility between ionic liquids having the tetrafluoroborate or hexafluorophosphate anion. The simulations show strong organization of CO$_2$ about hexafluorophosphate anions, but only small differences in CO$_2$ structure about the different cations. This is consistent with the experimental finding that, for a given anion, there are only small differences in CO$_2$ solubility for the two cations. Computed and measured densities, partial molar volumes, and thermal expansion coefficients are also reported.

1. Introduction

A number of investigations have shown that CO$_2$ is remarkably soluble in imidazolium-based ionic liquids.[1-5] We first investigated this phenomenon in connection with the possibility of extracting solutes from ionic liquids (ILs) with supercritical CO$_2$.[1,6] More detailed investigations showed that the anion and substituents on the cation did affect the CO$_2$ solubility somewhat, but the solubilities were quite high in all of the different ILs studied.[2] For instance, at just 50 bar of CO$_2$ pressure, the CO$_2$ solubility is on the order of 50 mol %.[2] Subsequent investigations at both low and high pressures have confirmed this behavior.[3-5]

As mentioned above, supercritical CO$_2$ can be used as an environmentally benign solvent to extract organic products or contaminants from ILs. This is a particularly attractive technique because the solubility of the IL in CO$_2$ is immeasurably low.[1] As a result, a number of researchers have adopted this methodology.[7-10] Obviously, understanding the phase behavior

of CO$_2$ with ILs is important for that application. We have also shown that CO$_2$ can be used to separate organic liquids and water from ILs by inducing a liquid—liquid phase split.[11,12] The amount of CO$_2$ dissolved in the IL/water or IL/organic mixture is key to determining how much CO$_2$ pressure is necessary to achieve the phase split. Finally, we have set forth the idea of using ILs for the separation of CO$_2$ from a wide variety of other gases.[13] Once again, the solubility of CO$_2$ in the various ILs is vital for the design and evaluation of gas separation processes using ILs. Therefore, we believe that it is important to gain a fundamental understanding of the mechanism for the high solubility of CO$_2$ in imidazolium-based ILs.

Kazarian and co-workers investigated mixtures of CO$_2$ with 1-*n*-butyl-3-methylimidazolium hexafluorophosphate ([bmim]-[PF$_6$]) and 1-*n*-butyl-3-methylimidazolium tetrafluoroborate ([bmim][BF$_4$]) using ATR-IR spectroscopy.[14] They found evidence of a weak Lewis acid—base interaction between the CO$_2$ and the anions of the ILs. The same group[15] used ATR-IR spectroscopy to probe IL/water solutions, which further confirmed the importance of interaction, in this case via hydrogen-bonding, of solutes with the anion. This was true for, among

(1) Blanchard, L. A.; Hancu, D.; Beckman, E. J.; Brennecke, J. F. *Nature* **1999**, *399*, 28−29.
(2) Blanchard, L. A.; Gu, Z. Y.; Brennecke, J. F. *J. Phys. Chem. B* **2001**, *105*, 2437−2444.
(3) Anthony, J. L.; Maginn, E. J.; Brennecke, J. F. *J. Phys. Chem. B* **2002**, *106*, 7315−7320.
(4) Kamps, A. P.-S.; Tuma, D.; Xia, J.; Maurer, G. *J. Chem. Eng. Data* **2003**, *48*, 746−749.
(5) Husson-Borg, P.; Majer, V.; Costa Gomes, M. F. *J. Chem. Eng. Data* **2003**, *48*, 480−485.
(6) Blanchard, L. A.; Brennecke, J. F. *Ind. Eng. Chem. Res.* **2001**, *40*, 287−292.
(7) Brown, R. A.; Pollet, P.; McKoon, E.; Eckert, C. A.; Liotta, C. L.; Jessop, P. G. *J. Am. Chem. Soc.* **2001**, *123*, 1254−1255.
(8) Liu, F.; Abrams, M. B.; Baker, R. T.; Tumas, W. *Chem. Commun.* **2001**, 433−434.
(9) Sellin, M. F.; Webb, P. B.; Cole-Hamilton, D. J. *Chem. Commun.* **2001**, 781−782.
(10) Lozano, P.; de Diego, T.; Carrie, D.; Vaultier, M.; Iborra, J. L. *Chem. Commun.* **2002**, 692−693.
(11) Scurto, A. M.; Aki, S.; Brennecke, J. F. *J. Am. Chem. Soc.* **2002**, *124*, 10276−10277.
(12) Scurto, A. M.; Aki, S. N. V. K.; Brennecke, J. F. *Chem. Commun.* **2003**, 572−573.
(13) Brennecke, J. F.; Maginn, E. J. U.S. Patent 6579343, 2003.
(14) Kazarian, S. G.; Briscoe, B. J.; Welton, T. *Chem. Commun.* **2000**, 2047−2048.
(15) Cammarata, L.; Kazarian, S. G.; Salter, P. A.; Welton, T. *Phys. Chem. Chem. Phys.* **2001**, *3*, 5192−5200.

other ILs, the interesting pair of 1-*n*-butyl-3-methylimidazolium hexafluorophosphate ([bmim][PF₆]) and 1-*n*-butyl-2,3-dimethylimidazolium hexafluorophosphate ([bmmim][PF₆]). For this second compound, the most acidic hydrogen on the imidazolium ring is replaced with a methyl group. Note that all of the imidazolium-based ILs for which CO_2 solubility has been measured previously possessed a hydrogen attached to the C2 carbon. The presence of acidic hydrogens on the imidazolium ring is particularly intriguing as a potential additional mechanism for CO_2 solvation. This speculation may seem reasonable based on the work of Welton and co-workers,[16] who used a series of solvatochromic dyes to determine the Kamlet−Taft parameters of various ILs. They found that the ability of imidazolium-based ILs to donate a hydrogen bond to solutes is significantly greater for salts possessing a hydrogen (rather than a methyl) attached to the C2 carbon.

Therefore, in this work, we seek to develop a comprehensive understanding of the mechanism of CO_2 dissolution in imidazolium-based ILs. We do this through a combined experimental and molecular simulation approach. Experimentally, we investigate the effects placing a methyl group versus a hydrogen at the 2-position on the imidazolium ring has on carbon dioxide solubility. We study three pairs of ILs: 1-*n*-butyl-3-methylimidazolium hexafluorophosphate ([bmim][PF₆]) and 1-*n*-butyl-2,3-dimethylimidazolium hexafluorophosphate ([bmmim][PF₆]); 1-*n*-butyl-3-methylimidazolium tetrafluoroborate ([bmim][BF₄]) and 1-*n*-butyl-2,3-dimethylimidazolium tetrafluoroborate ([bmmim][BF₄]); and finally 1-ethyl-3-methylimidazolium bis(trifluoromethylsulfonyl)imide ([emim][Tf₂N]) and 1-ethyl-2,3-dimethylimidazolium bis(trifluoromethylsulfonyl)imide ([emmim][Tf₂N]). Computationally, we use molecular dynamics simulations to examine mixtures of CO_2 with [bmim][PF₆] and [bmmim][PF₆]. We present a discussion of the experimental method and results first, followed by the simulation details and results.

2. Experimental Details

2.1. Materials. The [bmim][PF₆] was purchased from Sachem, with a reported halide content of less than 3 ppm. The [bmmim][PF₆], [bmim][BF₄], and [bmmim][BF₄] were obtained from the laboratory of Dr. Tom Welton at Imperial College, London. These samples were reported to contain less than 1.4 ppm residual halide.[15] The [emim][Tf₂N] and [emmim][Tf₂N] samples were 99+% electrochemical grade from Covalent Associates. All of the ionic liquid samples were dried in situ with the 10^{-9} bar vacuum of the gas absorption apparatus. The CO_2 was from Scott Specialty Gases with a purity of 99.99%.

The [bmmim][PF₆], [bmim][BF₄], and [bmmim][BF₄] were kept in an inert atmosphere, but were approximately 1 year old at the time of the experiments. Due to concerns that degradation products might have been present,[17] gas solubility experiments were repeated using fresh samples of [bmmim][PF₆] and [bmim][BF₄]. The [bmmim][PF₆] was obtained from Solvent Innovation. Because the sample was yellow upon receipt, it was mixed with activated carbon to remove most of the color. The [bmim][BF₄] was synthesized and purified in our lab and contained less than 8 ppm residual halide.[18] No differences in gas solubilities were observed between the fresh and old samples, so it was assumed that no degradation products that could affect gas solubility were present.

(16) Crowhurst, L.; Mawdsley, P. R.; Perez-Arlandis, J. M.; Salter, P. A.; Welton, T. *Phys. Chem. Chem. Phys.* **2003**, *5*, 2790−2794.
(17) Hardacre, C. 226th ACS National Meeting; New York, 2003.
(18) Fredlake, C. P.; Crosthwaite, J. C.; Hert, D. G.; Aki, S. N. V. K.; Brennecke, J. F. *J. Chem. Eng. Data* **2003**, submitted.
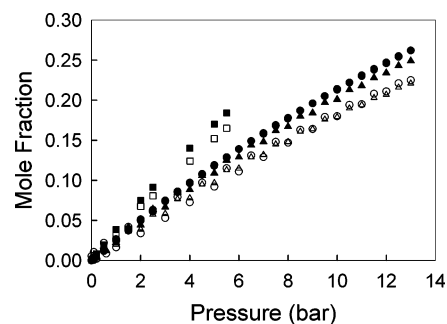
Figure 1. Solubility of CO_2 in [emim][Tf₂N], ■; [emmim][Tf₂N], □; [bmim][PF₆], ●; [bmmim][PF₆], ○; [bmim][BF₄], ▲; and [bmmim][BF₄], △ at 10 °C.
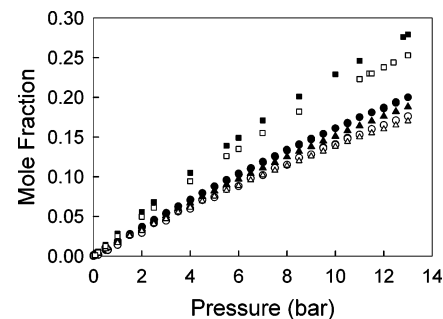
Figure 2. Solubility of CO_2 in [emim][Tf₂N], ■; [emmim][Tf₂N], □; [bmim][PF₆], ●; [bmmim][PF₆], ○; [bmim][BF₄], ▲; and [bmmim][BF₄], △ at 25 °C.

2.2. Method. The gas solubility measurements were made using a gravimetric microbalance (IGA 003, Hiden Analytical). A detailed description of this apparatus and the experimental procedure are given elsewhere.[3,19,20]

Analysis of the data from the microbalance requires accurate densities to account for buoyancy effects. Densities have been measured in our laboratory for the compounds investigated here and have been reported elsewhere.[18,21] Linear correlations of the densities as a function of temperature of each of the ILs were used here. These correlations are

$$[\text{bmim}][\text{PF}_6] \quad \rho(\text{g/cc}) = (-8.10 \times 10^{-4}) \times T(°C) + 1.38 \quad (1)$$

$$[\text{bmmim}][\text{PF}_6] \quad \rho(\text{g/cc}) = (-1.37 \times 10^{-3}) \times T(°C) + 1.27 \quad (2)$$

$$[\text{bmim}][\text{BF}_4] \quad \rho(\text{g/cc}) = (-6.43 \times 10^{-4}) \times T(°C) + 1.22 \quad (3)$$

$$[\text{bmmim}][\text{BF}_4] \quad \rho(\text{g/cc}) = (-1.27 \times 10^{-3}) \times T(°C) + 1.13 \quad (4)$$

$$[\text{emim}][\text{Tf}_2\text{N}] \quad \rho(\text{g/cc}) = (-9.61 \times 10^{-4}) \times T(°C) + 1.54 \quad (5)$$

$$[\text{emmim}][\text{Tf}_2\text{N}] \quad \rho(\text{g/cc}) = (-9.09 \times 10^{-4}) \times T(°C) + 1.51 \quad (6)$$

3. Experimental Results and Discussion

The solubility isotherms at 10, 25, and 50 °C for each of the six ionic liquids are shown in Figures 1−3, respectively. All data collected, including absorption and desorption, have been plotted. At 10 °C, there is slight hysteresis between the absorption and desorption for [bmmim][PF₆] and [bmmim][BF₄], which is reflected in larger uncertainties in the Henry's law constants shown in Table 1. It should be noted that at both 10 and 25 °C, some of the ionic liquids are subcooled liquids.[18]

(19) Macedonia, M. D.; Moore, D. D.; Maginn, E. J.; Olken, M. M. *Langmuir* **2000**, *16*, 3823−3834.
(20) Anthony, J. L.; Maginn, E. J.; Brennecke, J. F. *J. Phys. Chem. B* **2001**, *105*, 10942−10949.
(21) Gu, Z. Y.; Brennecke, J. F. *J. Chem. Eng. Data* **2002**, *47*, 339−345.
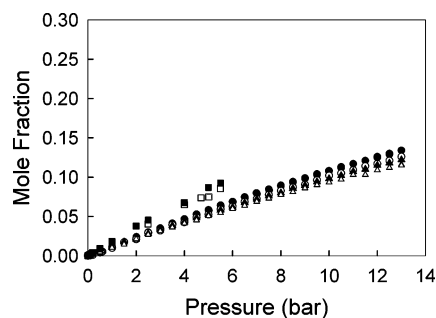
Figure 3. Solubility of CO_2 in [emim][Tf$_2$N], ■; [emmim][Tf$_2$N], □; [bmim][PF$_6$], ●; [bmmim][PF$_6$], ○; [bmim][BF$_4$], ▲; and [bmmim][BF$_4$], △ at 50 °C.

Table 1. Experimental Henry's Constants at Three Temperatures and Enthalpies and Entropies of Dissolution for CO_2 Dissolved in the Six Ionic Liquids

	H (bar)				
ionic liquid	10 °C	25 °C	50 °C	Δ*h* (kJ/mol)	Δ*s* (J/mol K)
[bmim][PF$_6$]	38.7 ± 0.4	53.4 ± 0.3	81.3 ± 0.5	−16.1 ± 2.2	−53.2 ± 6.9
[bmmim][PF$_6$]	47.3 ± 7.5	61.8 ± 2.1	88.5 ± 1.8	−13.0 ± 1.3	−42.8 ± 9.8
[bmim][BF$_4$]	40.8 ± 2.7	56.5 ± 1.4	88.9 ± 3.2	−15.9 ± 1.3	−52.4 ± 4.3
[bmmim][BF$_4$]	45.7 ± 3.4	61.0 ± 1.6	92.2 ± 1.2	−14.5 ± 1.4	−47.7 ± 4.4
[emim][Tf$_2$N]	25.3 ± 1.3	35.6 ± 1.4	51.5 ± 1.2	−14.2 ± 1.6	−46.9 ± 3
[emmim][Tf$_2$N]	28.6 ± 1.2	39.6 ± 1.4	60.5 ± 1.5	−14.7 ± 1.2	−48.7 ± 4

Visual observations before and after the gas solubility measurements, however, indicate that the samples remained liquid on experimental time scales. In the figures, the ionic liquids with a hydrogen attached to the 2-carbon are shown using filled symbols, while the ILs with a methyl group substituted in the 2-position are shown using open symbols. At all temperatures, the ILs with the [Tf$_2$N] anion show the highest CO_2 solubility, whereas there is little difference between the CO_2 solubilities in the [BF$_4$] versus [PF$_6$] based ILs. The effect temperature has on the solubility difference between the methyl-substituted and hydrogen-substituted ILs suggests that this substitution induces some change in the energetic interactions between CO_2 and the cation. At 10 °C (Figure 1), there is some decreased solubility for the methyl-substituted IL relative to the hydrogen-substituted IL in each pair, particularly at higher pressures. As the temperature is increased, the discrepancy between the CO_2 solubility in each of the three pairs of ILs decreases so that at 50 °C there is very little difference between the two ILs (Figure 3). However, this trend is less dramatic with the more CO_2-philic [emim][Tf$_2$N] and [emmim][Tf$_2$N] compounds. This suggests that the interactions governing the higher solubility of CO_2 in the [Tf$_2$N] ILs are not influenced as strongly by the presence of a hydrogen or methyl group on the C2 carbon.

Table 1 lists Henry's constants (*H*) in bar for the six ionic liquids, each at 10, 25, and 50 °C. Henry's constant, as defined in this work, is

$$H = \lim_{x \to 0} \frac{p}{x} \tag{7}$$

where *x* is the limiting mole fraction of CO_2 absorbed in the ionic liquid and *p* is the pressure of CO_2 in the gas phase. The gas phase is assumed to be pure and ideal, both of which are excellent assumptions under the conditions investigated. Equation 7 implies that a smaller value for the Henry's constant indicates a larger gas solubility. For all three pairs, the presence

of the methyl group slightly decreases the CO_2 solubility, but the overall effect is minor. This indicates that the presence of the hydrogen at the 2-position only has a small impact on the CO_2 solubility. Therefore, other factors are responsible for the high CO_2 solubility observed in these ILs.

The error reported for Henry's constants is determined by using the absorption and desorption isotherms as the upper and lower bounds for the true equilibrium value.[3] The data were fit to a quadratic function, and the limiting slope was found analytically. The reproducibility between different IL samples is approximately 1−3%; typically, this deviation is within the error bars determined from the absorption/desorption hysteresis. For [bmim][BF$_4$] at 25 and 50 °C, the standard deviation between samples was slightly larger than the deviation between absorption and desorption Henry's constants. Therefore, the larger of the two deviations was reported as the experimental error.

Further evidence of the limited influence of the hydrogen in the 2-position can be obtained by examining the enthalpy (Δ*h*$_1$) and entropy (Δ*s*$_1$) of absorption, as reported in Table 1. These changes are calculated by

$$\Delta h_1 = \bar{h}_1 - h_1^{ig} = R\left(\frac{\partial \ln p}{\partial(1/T)}\right)_{x_1} \tag{8}$$

$$\Delta s_1 = \bar{s}_1 - s_1^{ig} = -R\left(\frac{\partial \ln p}{\partial \ln T}\right)_{x_1} \tag{9}$$

where $\bar{h}_1$ and $\bar{s}_1$ are the partial molar enthalpy and entropy of gas in solution, h_1^{ig} and s_1^{ig} are the enthalpy and entropy of the pure gas in the ideal gas phase, *p* is the partial pressure of the gas, *T* is the temperature of the system, and x_1 is the mole fraction of gas dissolved in the IL. Information about the strength of interaction between the IL and gas is provided by the enthalpy, while information about the degree of ordering that takes place upon dissolution of the gas is given by the entropy. Within the reported error, we found that the calculated values of Δ*h*$_1$ and Δ*s*$_1$ were independent of composition (x_1) and equal to the infinite dilution values, as found from the van't Hoff equations.[3,20]

The experimental enthalpies and entropies for the [Tf$_2$N] ILs, which also had the highest CO_2 solubility, are the same regardless of the presence of the methyl group. For the [PF$_6$] and [BF$_4$] ILs, it is difficult to draw a definite conclusion because the enthalpies and entropies are very close within the reported error. Because only three temperatures were examined, the experimental uncertainty is relatively large. Despite this, it does appear that the enthalpies for the ILs with the methyl group substituted on the second carbon are lower by 1−3 kJ/mol.

On the basis of these findings, we conclude that the presence of a hydrogen on the C2 carbon affects the CO_2 solubility only slightly; it plays a very small role in determining the overall high solubility of CO_2 in imidazolium-based ILs. The results show instead that CO_2 solubility is affected much more by the nature of the anion; the ILs with the [Tf$_2$N] anion had a much greater CO_2 solubility than those with either the [PF$_6$] or the [BF$_4$] anions. This may be due to the fact that the [Tf$_2$N] anion contains two fluoroalkyl groups, which are known to increase CO_2 solubility in other fluids. These results are entirely consistent with the ATR-IR studies that showed that CO_2 solubility in [bmim][PF$_6$] and [bmim][BF$_4$] is governed by

interactions with the anion.[14] To obtain additional insight into the interactions between CO$_2$ and the ILs, molecular modeling was used to examine the structure of the IL/CO$_2$ mixtures.

4. Simulation Details

Molecular dynamics simulations in the isothermal−isobaric ensemble were conducted using the program NAMD.[22] Pressure was maintained at the desired set point by means of a modified Nosé−Hoover method in which Langevin dynamics were used to control fluctuations in the barostat. The barostat oscillation time and damping factors were set to 1 ps. Temperature was maintained via Langevin dynamics with a damping factor of 5 ps^{-1}. The simulation time step was 1 fs.

Simulations were conducted on the pure ionic liquids at 0.98 bar and temperatures of 25, 50, and 70 °C using 90 cations and 90 anions. Results of these calculations were used to compute densities and coefficients of thermal expansion. They were also compared with our previous simulation results for [bmim][PF$_6$] at these conditions,[23,24] to assess the effect small differences in the intermolecular force field between this work and the previous study had on the computed properties. Very little difference was observed. Pure [bmim][PF$_6$] and a mixture of 90 [bmim] cations, 90 [PF$_6$] anions, and 10 CO$_2$ molecules were simulated at 25 °C and 5.3 bar. Similar calculations were made for pure [bmmim][PF$_6$] and a [bmmim][PF$_6$]/CO$_2$ mixture at 25 °C and 6.18 bar. These conditions were chosen to match as closely as possible experimental isotherm results (see Figure 2), which indicate that the mole fraction of CO$_2$ in the different ILs is 10 mol % at the two respective pressures. The small but finite concentration of CO$_2$ in the liquid phase permits the examination of the organization of CO$_2$ within the liquid, thus shedding light on how CO$_2$ interacts with the different ILs.

Initial configurations for the pure and mixture simulations were obtained by randomly placing molecules in the simulation box and rejecting any configurations that had significant overlap.[23] Once all of the molecules were added to the box, a conjugant-gradient energy minimization was performed, followed by a 100 ps MD simulation and a second energy minimization. This system was then simulated for 2 ns, with data collected only over the last 1 ns.

The force field used in this work has the functional form

$$U_{\text{tot}} = \sum_{\text{bonds}} k_b (r - r_o)^2 + \sum_{\text{angles}} k_\theta (\theta - \theta_o)^2 +$$
$$\sum_{\text{dihedrals}} k_\chi [1 + \cos(n\chi - \delta)] + \sum_{\text{improper}} k_\psi (\psi - \psi_o)^2 +$$
$$\sum_{i=1}^{N-1} \sum_{j>i}^{N} \left\{ 4\epsilon_{ij} \left[\left(\frac{\sigma_{ij}}{r_{ij}} \right)^{12} - \left(\frac{\sigma_{ij}}{r_{ij}} \right)^6 \right] + \frac{q_i q_j}{r_{ij}} \right\} \quad (10)$$

where the symbols have their conventional meaning.[25] The dispersion−repulsion interactions were cut off by multiplying the Lennard-Jones potential by a switching function parameter of the following form

$$\eta_{\text{SF}}(r_{ij}) =$$
$$\begin{cases} 1 & \text{if } |r_{ij}| \le r_s \\ \dfrac{(r_c^2 - |r_{ij}|^2)^2 (r_c^2 + 2|r_{ij}|^2 - r_s^2)}{(r_c^2 - r_s^2)^2} & \text{if } r_s < |r_{ij}| \le r_c \quad (11) \\ 0 & \text{if } |r_{ij}| > r_c \end{cases}$$

where r_c is the potential cutoff of 1.2 nm and r_s is the onset distance for the switching function, set to 1.05 nm. A particle mesh Ewald sum was used for handling electrostatics. Intramolecular Lennard-Jones and Coulombic interactions between atoms separated by less than three bonds were neglected. Coulombic interactions between atoms separated by three bonds were scaled by a factor of 0.4, while Lennard-Jones interactions for these atoms were fully considered. Atoms separated by more than three bonds were allowed to interact at full strength.

Force field parameters for eq 10 were obtained in the following manner. Lennard-Jones parameters for all of the cation and anion atom types were obtained from the CHARMM 27 force field[26] using imidazole as a basis for the imidazolium atoms. Lennard-Jones parameters for CO$_2$ were taken from the TraPPE force field.[27] Partial charges for the cations and anions were obtained by performing ab initio calculations on an isolated cation−anion pair. Three energy-minimized structures were obtained from calculations at the B3LYP/6-311+G* level of theory. Partial charges for each structure were obtained using the CHELPG method,[28] and averages of these charges were used in the subsequent MD simulations. In contrast to our previous study,[23] symmetry of charge for equivalent atoms was enforced, thus resulting in a slightly modified force field. The partial charges for CO$_2$ were taken directly from the TraPPE model.[27] Nominal bond lengths and bond angles for each IL species were obtained from ab initio energy-minimized structures of the ions in the gas phase. The experimental bond length for CO$_2$ was used.[29] With the exception of the bond and angle force constants for [PF$_6$] and CO$_2$, all harmonic force constants in eq 10 were taken from CHARMM. The remaining force constants were determined from the ab initio calculations by perturbing the appropriate internal coordinate of a single [PF$_6$] or CO$_2$ a small amount, computing the energy change, and relating this to the appropriate harmonic energy term. Torsion angle potential parameters, when available, were obtained directly from CHARMM. For those torsion angles not explicitly included in CHARMM, substitutions based on related compounds were used. A complete listing of all force field parameters, along with a listing of these substitutions, is provided in the Supporting Information (Table S.1).

5. Simulation Results and Discussion

5.1. Liquid Properties. Pure [bmim][PF$_6$] and [bmmim][PF$_6$] were simulated at 0.98 bar and 25, 50, and 70 °C. Densities and coefficients of thermal expansion were computed and compared to experimental values[18,21] (see Table 2). The [bmim]-[PF$_6$] densities are consistent with the previous simulations,[23] as expected given the relatively small changes in the force field between the two studies. Simulated densities are roughly 2% lower than experimental values for [bmim][PF$_6$], but are 4−6% higher than the experimental values for [bmmim][PF$_6$]. [bmmim]-

(22) Kale, L.; Skeel, R.; Bhandarkar, M.; Brunner, R.; Gursoy, A.; Krawetz, N.; Phillips, J.; Shinozaki, A.; Varadarajan, K.; Schulten, K. *J. Comput. Phys.* **1999**, *151*, 283−312.
(23) Morrow, T. I.; Maginn, E. J. *J. Phys. Chem. B* **2002**, *106*, 12807−12813.
(24) Morrow, T. I.; Maginn, E. J. *J. Phys. Chem. B* **2003**, *107*, 9160.
(25) Allen, M. P.; Tildesley, D., J. *Computer Simulations of Liquids*; Clarendon: Oxford, 1987.
(26) Mackerell, A. D.; Wiorkiewicz-Kuczera, J.; Karplus, M. *J. Am. Chem. Soc.* **1995**, *117*, 11946.
(27) Potoff, J. J.; Siepmann, J. I. *AIChE J.* **2001**, *47*, 1676−1682.
(28) Breneman, C. M.; Wiberg, K. B. *J. Comput. Chem.* **1990**, *11*, 361−373.
(29) Lide, D. R. *CRC Handbook of Chemistry and Physics*, 74th ed.; CRC Press: Boca Raton, FL, 1993.

Table 2. Experimental and Simulated Densities and Coefficients of Thermal Expansion as a Function of Temperature at 0.98 bar

[bmim][PF$_6$]

T °C	ρ_{expt}[21] (g/cm³)	ρ_{sim} (g/cm³)	$\alpha_{P,expt}$ (×10⁴ K⁻¹)	$\alpha_{P,sim}$ (×10⁴ K⁻¹)
25	1.360	1.326	6.0	5.2
30	1.356			
40	1.349			
50	1.340	1.310		
60	1.332			
70	1.324	1.295		

[bmmim][PF$_6$]

T °C	ρ_{expt}[18] (g/cm³)	ρ_{sim} (g/cm³)	$\alpha_{P,expt}$ (×10⁴ K⁻¹)	$\alpha_{P,sim}$ (×10⁴ K⁻¹)
22.5	1.242		10.7	5.9
25	1.236*	1.282		
40	1.219			
50	1.206	1.267		
70	1.174*	1.249		

[a] The experimental densities having a "*" were estimated from the correlation given by eq 2. Values of the coefficient of thermal expansion are averages over the entire temperature range.

[PF$_6$] has a significantly lower density than [bmim][PF$_6$], which suggests that the extra methyl group on the [bmmim] cation reduces the packing efficiency of the fluid, thereby lowering the density. This trend is captured by the simulations, although the magnitude of the density change is underpredicted. The volume of the fluid expands in a nearly linear fashion with increasing temperature over the range examined here. The simulated coefficient of thermal expansion for [bmim][PF$_6$] is 5.2×10^{-4} K⁻¹, while the experimental value is 6.0×10^{-4} K⁻¹. For [bmmim][PF$_6$], the simulated value is 5.9×10^{-4} K⁻¹; however, the experimental coefficient is significantly larger at 10.7×10^{-4} K⁻¹. The experiments indicate that the addition of the methyl group on the C2 position has a dramatic effect on the coefficient of thermal expansion for [bmmim][PF$_6$], increasing it by almost 80% over the [bmim] counterpart. The simulations predict a much more modest 13% increase. It is not clear why the models underestimate the temperature dependence of density, nor is it apparent why the deviation between simulations and experiment is so much larger for [bmmim][PF$_6$] than for [bmim][PF$_6$]. Part of the reason could be that the calculated coefficients of thermal expansion are small numbers calculated from differences in large numbers and are thus difficult to obtain accurately. Nevertheless, both the simulations and the experiments indicate that [bmmim][PF$_6$] has a larger coefficient of thermal expansion than [bmim][PF$_6$]. This is consistent with the physical picture that the [bmmim] cation enables less efficient packing than the [bmim] cation and thus expands more upon heating. Note that the large difference in experimental coefficients of thermal expansion is also seen for [bmmim][BF$_4$] and [bmim][BF$_4$], but is not observed for [emmim][Tf$_2$N] and [emim][Tf$_2$N]. The qualitatively different behavior observed for the [Tf$_2$N] compounds could be due to either a weaker association between the [Tf$_2$N] anion and the cations or packing differences between ethyl- and butyl-substituted imidazolium cations.

Experimental isothermal compressibilities, κ_T, are 2.7×10^{-5} bar⁻¹ for [bmim][PF$_6$][21] and have not been measured for the other five ILs to our knowledge. Because κ_T is so small and the simulations were performed over a relatively small pressure

range, a reliable estimate for κ_T was not obtained from the simulations.

To examine how much the liquid expands upon addition of CO$_2$, the partial molar volume of CO$_2$ in [bmim][PF$_6$] and [bmmim][PF$_6$] was calculated. Using experimental data from our laboratory,[30] we found that at CO$_2$ mol fractions below 0.49, the partial molar volume of CO$_2$ is nearly constant at 29 cm³/mol, while the simulations predict a value of 33 cm³/mol at the one concentration examined, 10 mol % CO$_2$. The partial molar volumes for the ionic liquid remain essentially equal to their pure component values, confirming that the CO$_2$ does not greatly perturb the underlying structure of the ionic liquid. This conclusion is supported by the mixture simulation results described below. The computed partial molar volume for CO$_2$ in [bmim][PF$_6$] is 28 cm³/mol, which is slightly smaller than that for [bmim][PF$_6$]. No experimental values for [bmmim][PF$_6$] are available. The partial molar volumes for CO$_2$ in three common organic solvents, calculated from solubility data in the literature at 25 °C,[31] are 34 for acetonitrile, 79 for ethyl acetate, and 47 cm³/mol for ethanol. In general, the partial molar volumes for CO$_2$ in conventional organic solvents are larger than those seen for the ionic liquids. This difference is consistent with the smaller degree of volume expansion upon dissolution seen in ILs relative to other organics.[2] These results indicate that the physical picture of these liquids is that of the anions and cations forming a strong network with the CO$_2$ filling the interstices in the fluid, with the strongest interactions occurring about the [PF$_6$] anion.

In principle, the simulations can also yield an estimate of the enthalpy of absorption for CO$_2$. This can be done by taking the difference in the molar enthalpy of the neat liquid and of that having 10 mol % CO$_2$. Unfortunately, the uncertainties associated with this calculation make the estimates of little value. For example, the enthalpy of solvation for CO$_2$ in [bmim][PF$_6$] was calculated as -18 ± 26 kJ/mol, while in [bmmim][PF$_6$] it was -23 ± 27 kJ/mol. The large uncertainty in these values stems from the fact that they are computed as small differences between large numbers. The strong energetics arising from the Coulombic interactions lead to these large energy terms, whose fluctuations are on the order of the enthalpies of interest. A more accurate estimate may be obtained by computing the temperature dependence of the free energy of absorption, which is the subject of future work.

5.2. Pure Liquid Structure. As discussed in the Introduction, previous studies[16,23] have indicated that the hydrogen attached to the C2 carbon on the [bmim] cation is "acidic" (i.e., it has a relatively large positive charge) and adds significantly to the hydrogen bonding ability of the cation. This suggests that the [PF$_6$] anion should associate strongly with this site, which has been confirmed in previous experimental,[32] ab initio,[33,34] and classical simulation studies.[23,35,36] Because this site is replaced by a methyl group in [bmmim], one expects that the anion

(30) Aki, S. N. V. K.; Sauer, E. M.; Brennecke, J. F. 2004, manuscript in preparation.
(31) Kordikowski, A.; Schenk, A. P.; VanNielen, R. M.; Peters, C. J. *J. Supercrit. Fluids* **1995**, *8*, 205−216.
(32) Hardacre, C.; McMath, S. E. J.; Nieuwenhuyzen, M.; Bowron, D. T.; Soper, A. K. *J. Phys.: Condens. Matter* **2003**, *15*, S159−S166.
(33) Morrow, T. I.; Maginn, E. J. In *Ionic Liquids*; Seddon, K. R., Rogers, R. D., Eds.; American Chemical Society: Washington, DC, 2003.
(34) Meng, Z.; Dolle, A.; Carper, W. R. *THEOCHEM* **2002**, *585*, 119−128.
(35) Hanke, C. G.; Price, S. L.; Lynden-Bell, R. M. *Mol. Phys.* **2001**, *99*, 801−809.
(36) Shah, J. K.; Maginn, E. J. *Fluid Phase Equilib.*, 2003, submitted.
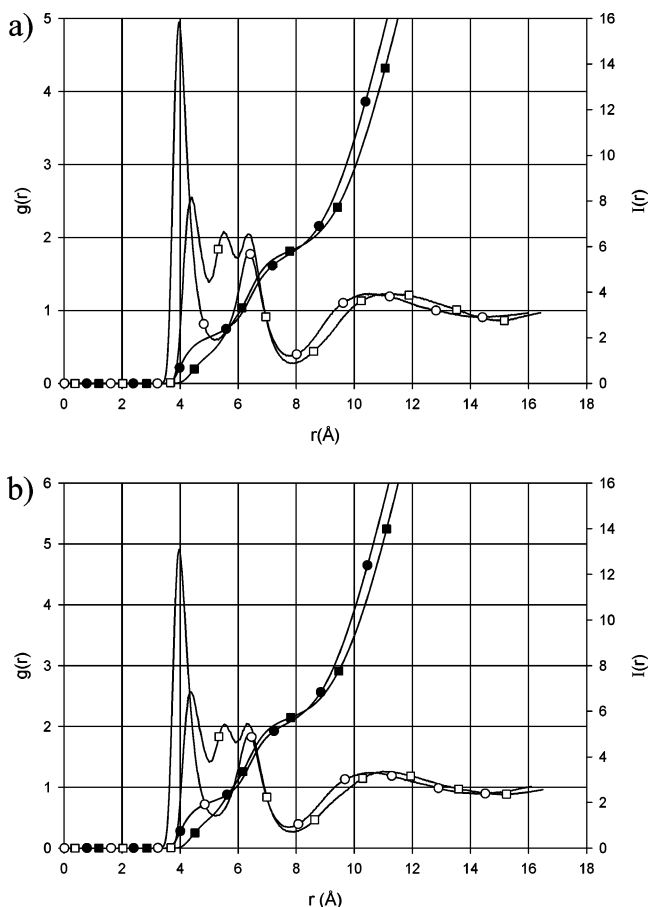
Figure 4. (a) Radial distribution functions and number integrals for the phosphorus atom of the [PF₆] anion about the C2 carbon of the cation. Symbol meanings: $g(r)$ for [bmim], ○; $g(r)$ for [bmmim], □; $I(r)$ for [bmim], ●; $I(r)$ for [bmmim], ■. (b) The same plots and symbol meanings as in (a), except with 10 mol % CO₂. The CO₂ has no perceptible change in the ordering of the cation and anion.

distribution will be altered for this IL relative to the [bmim] case. Both the ab initio and the MD simulations confirm this expectation. In the ab initio calculations for the cation–anion pairs, the minimum energy conformation for [bmim][PF₆] always involved [PF₆] associating with the C2 carbon, regardless of the starting configuration. For [bmmim][PF₆], however, local minima were found in which the [PF₆] anion localized on both sides of the imidazolium ring. The organization of the bulk liquid can best be analyzed in a condensed phase MD simulation by examining various site–site radial distribution functions, $g(r)$, and site–site number integrals, $I(r)$. Each $g(r)$ represents the distance-dependent relative probability of observing a given site or atom relative to some central site or atom. $I(r)$ is simply the average number of specific sites or atoms within a sphere of radius r about some other central site or atom. In general, there are two $I(r)$ plots for each pair of sites investigated, unless there are an equal number of sites, in which case the two plots are equal.

Figure 4a shows $g(r)$ and $I(r)$ for the phosphorus atom of the [PF₆] anion and the C2 carbon of the imidazolium ring in [bmim] and [bmmim]. For [bmim], a sharp, intense peak in $g(r)$ is observed at about 4 Å. Broader peaks at 6.5 Å and roughly 10 Å are also observed. In contrast, $g(r)$ for [bmmim] has three weaker peaks at distances ranging from 4.5 to 6.5 Å. The peak at the shortest distance represents the direct association of [PF₆]
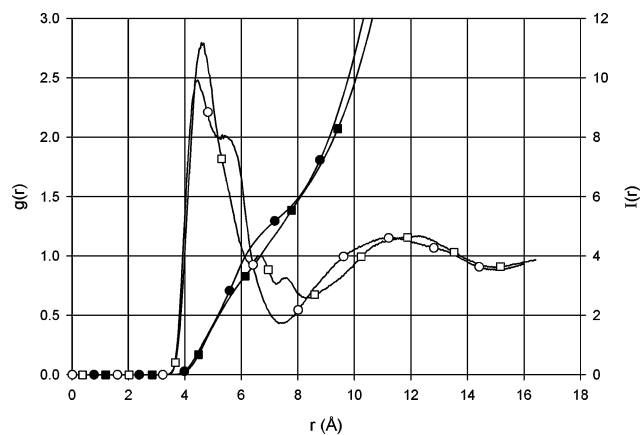
Figure 5. Radial distribution functions and number integrals for the phosphorus atom of [PF₆] about the C4 carbon atom of the two different cations. Symbol meanings: $g(r)$ for [bmim], ○; $g(r)$ for [bmmim], □; $I(r)$ for [bmim], ●; $I(r)$ for [bmmim], ■.

with the C2 carbon, while the other two peaks result from interactions of the [PF₆] located elsewhere with respect to the cation. The fact that the intensity of the closest C2 peak is greatly reduced relative to [bmim] confirms that the replacement of the hydrogen with the methyl group reduces the tendency of [PF₆] to organize about the C2 site on the ring. The first peak in the [bmim] $g(r)$ is at a shorter distance than that for [bmmim], which reflects the 0.6–0.7 Å screening length of the methyl group on the C2 carbon of [bmmim]. This screening length is also apparent in the number integrals. For [bmim], $I(r) = 1$ at 4.1 Å and $I(r) = 2$ at 5.0 Å, while for [bmmim], these distances are 4.8 and 5.5 Å, respectively. Figure 4b shows the same functions but with the addition of 10 mol % CO₂. By comparing with Figure 4a, it can be seen that CO₂ has a negligible effect on the organization of [PF₆] about the C2 carbon. Other distribution functions also show little or no change upon addition of 10 mol % CO₂, indicating that the overall organization of the liquid is relatively unperturbed by the addition of CO₂. This is due to the strong Coulombic interactions responsible for the organization of the liquid, which help form a network in which dissolving CO₂ is forced to locate in the interstices. This physical picture of gas absorption is consistent with the observation that the volume of these ILs changes very little upon addition of relatively large amounts of CO₂, as discussed above.

It may be expected that because the C2 site is blocked in [bmmim] but not in [bmim], the anion order on the C4 and C5 sides of these cations would differ. The simulation results, however, suggest that there is very little difference. Figure 5 shows $g(r)$ and $I(r)$ for the organization of [PF₆] about the C4 carbon of the two cations. Results for [PF₆] and C5 are qualitatively similar. The first peak in the $g(r)$ for [bmmim] occurs at the same distance as for [bmim] and is only slightly higher. For both liquids, $I(r) = 1$ at 4.7 Å and $I(r) = 2$ at 5.2 Å. The shoulder in $g(r)$ starting at 5.5 Å for [bmim] is from residual order induced by the strong association of a second anion about the C2 position. Long-range organization (beyond 10 Å) is also similar for both liquids. The small difference in $I(r)$ for the two liquids beyond 10 Å is due to the fact that [bmmim][PF₆] has a lower bulk density than [bmim][PF₆]. Most interesting is the fact that the first peak in the [bmim][PF₆] $g(r)$ is greatly reduced and broadened relative to the first $g(r)$ peak for anion–C2 association shown in Figure 4a, again emphasiz-

a)

b)
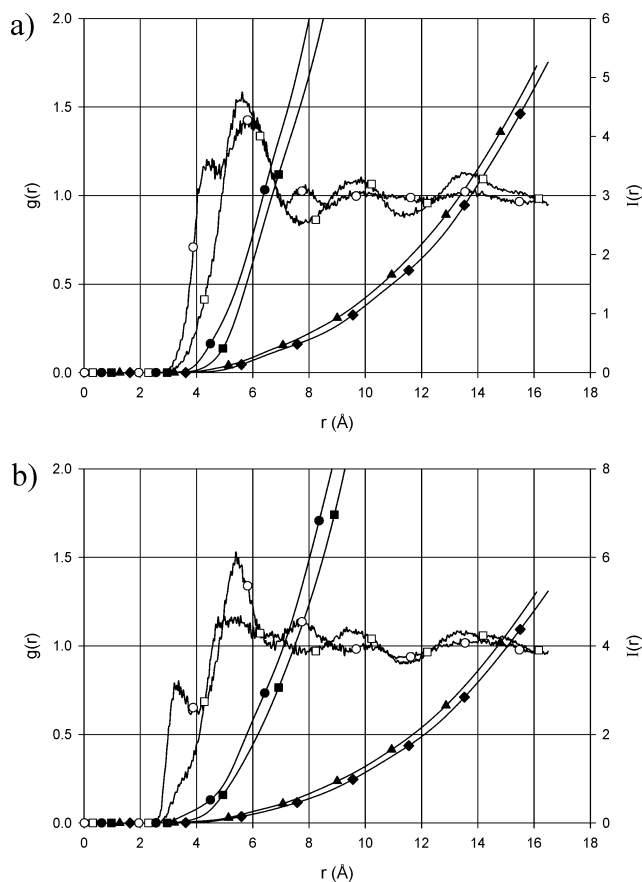
Figure 6. (a) Radial distribution functions and number integrals for the carbon atom of CO_2 and the C2 carbon atom of the two cations. (b) Same plot as (a), but for the oxygen atom of CO_2 and the C2 carbon atom of the cations. Symbol meanings: $g(r)$ for [bmim], ○; $g(r)$ for [bmmim], □; $I(r)$ for [bmim] C2 carbon about the CO_2 carbon (a) or oxygen (b) atom, ●; $I(r)$ for [bmmim] C2 carbon about the CO_2 carbon (a) or oxygen (b) atom, ■; $I(r)$ for the CO_2 carbon (a) or oxygen (b) about the C2 carbon of [bmim], ▲; $I(r)$ for the CO_2 carbon (a) or oxygen (b) about the C2 carbon of [bmmim], ◆.

ing the much stronger organization of the anion about the C2 carbon in this liquid.

5.3. Mixture Liquid Structure. While the addition of a methyl group at the C2 position alters the organization of the anion about the cation, the mixture simulation results show that this change has a much smaller effect on the organization of CO_2 about the cation. Figure 6a shows $g(r)$ and $I(r)$ for the interaction of the CO_2 carbon atom with the C2 carbon atom of the imidazolium ring, while Figure 6b is the same plot for one oxygen atom of CO_2 and the C2 carbon. Both initial $g(r)$ peaks are broad and of low intensity, indicating a relatively weak organization of CO_2 about the C2 carbon. Both plots have a split first peak for the [bmim] cation, with the closest "shoulder" peak being of lower intensity than the second peak. For the [bmmim] cation, only one initial peak is observed. This indicates that CO_2 takes on two orientations with respect to the C2 position of [bmim] but only one for [bmmim]. The initial shoulders in the [bmim] case are at roughly 3.2 Å for oxygen and 4.2 Å for carbon, indicating that some configurations are in an "end-on" orientation in which the oxygen atom directly associates with the hydrogen at the C2 position. The remaining configurations are further away and suggest a more orientationally averaged conformation, similar to that observed for the [bmmim] cation. The number integrals also show the screening

a)

b)
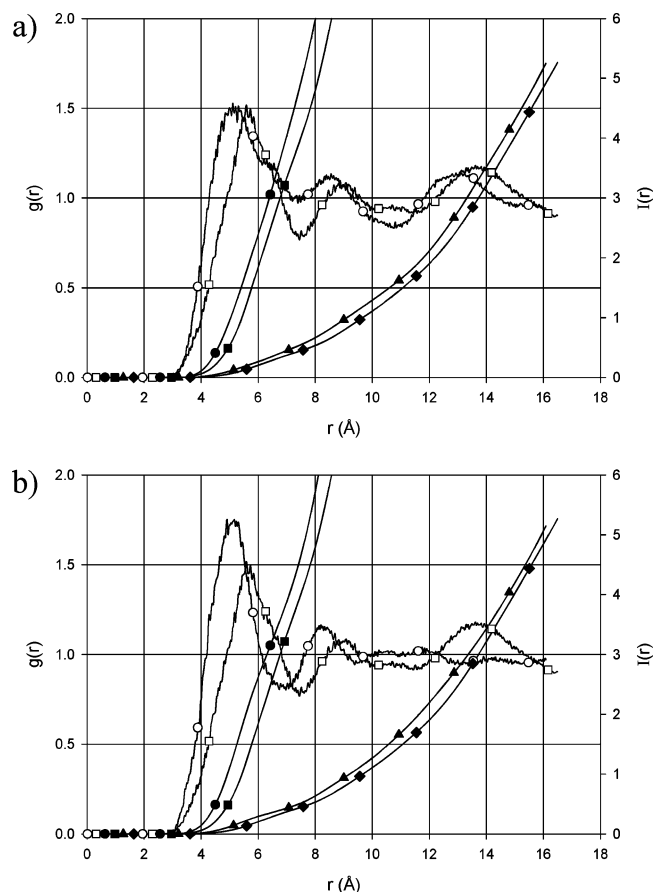
Figure 7. Radial distribution functions and number integrals for CO_2 and the N1 nitrogen of the cation (a) and N3 nitrogen of the cation (b). Symbol meanings: $g(r)$ for [bmim], ○; $g(r)$ for [bmmim], □; $I(r)$ for [bmim] nitrogen about the CO_2 carbon, ●; $I(r)$ for [bmmim] nitrogen about the CO_2 carbon, ■; $I(r)$ for the CO_2 carbon about the nitrogen of [bmim], ▲; $I(r)$ for the CO_2 carbon about the nitrogen of [bmmim], ◆.

effect of the methyl group on [bmmim]; for the C2 carbon on [bmim] about a central CO_2 carbon, $I(r) = 1$ at 5.1 Å and $I(r) = 2$ at 5.8 Å, while for [bmmim] these distances are 5.5 and 6.1 Å, respectively. Note that there are two number integrals in this figure for each pair, due to the fact that there are more C2 carbons in the system than CO_2 molecules. At long distances, the individual $I(r)$ plots approach the total number of sites surrounding the central site in a sphere of the appropriate radius.

Interestingly, a similar screening effect is observed between CO_2 and the nitrogens on the cations. Figure 7a shows that the first $g(r)$ peak for CO_2–N1 occurs at a slightly smaller distance for the [bmim] cation than for the [bmmim] cation. For [bmim], $I(r) = 1$ at 5.0 Å and $I(r) = 2$ at 5.7 Å, while for [bmmim] these distances are 5.4 and 6.0 Å, respectively. For the N3 position, the situation is similar. Figure 7b indicates that CO_2 is able to locate closer to the N3 of the [bmim] cation than the [bmmim] cation. $I(r) = 1$ at 4.9 Å and $I(r) = 2$ at 5.5 Å for [bmim], while for [bmmim] these distances are 5.4 and 6.1 Å, respectively. This can be understood by the fact that N3 has a relatively large positive partial charge of 0.199 in the [bmim] case, but a charge of only 0.034 for [bmmim]. In addition, the two methyl groups attached to the N3 and C2 carbons in the [bmmim] cation may shield the N3 position more effectively than the hydrogen attached to C2 and the single methyl group attached to N3 for the [bmim] cation.
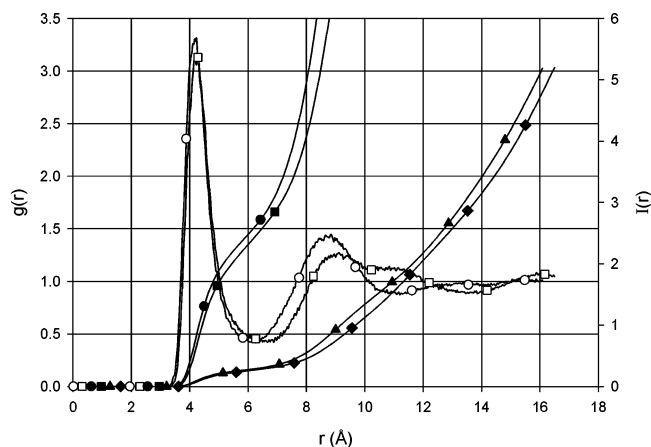
Figure 8. Radial distribution functions and number integrals for the carbon atom of CO_2 and the phosphorus atom of $[PF_6]$. Symbol meanings: $g(r)$ for [bmim], ○; $g(r)$ for [bmmim], □; $I(r)$ for phosphorus atom of [bmim]-$[PF_6]$ about the CO_2 carbon, ●; $I(r)$ for phosphorus atom of $[bmmim][PF_6]$ about the CO_2 carbon, ■; $I(r)$ for the CO_2 carbon about the phosphorus atom of $[bmim][PF_6]$, ▲; $I(r)$ for the CO_2 carbon about the phosphorus of $[bmmim][PF_6]$, ◆.

Although the above results suggest that the addition of a methyl group to the cation changes the organization of CO_2 in the liquid, these changes should have a small effect on overall solubility. This is because most of the CO_2 is located relatively far away from the cations (ca. 5 Å or more). Subtle differences of 0.2−0.4 Å in interaction distance will not result in large enough energetic differences to influence solubility to a great deal. This is consistent with the experimental observation that CO_2 solubility differences between these two cations is small.

In contrast to the relatively weak organization observed for CO_2 about the major cation positions, Figure 8 shows the strong association between the carbon atom of CO_2 and the phosphorus atom of $[PF_6]$ anion. The first $g(r)$ peak is sharp and much more intense than those observed for CO_2 and the C2 carbon atom of the cations. $I(r) = 1$ at 4.3 Å for [bmim] and 4.4 Å for [bmmim], which is nearly 1 Å closer than the comparable number integrals for the CO_2 carbon and the cation C2 carbon. Furthermore, the average distance at which two anions associate with a CO_2 carbon is 5.1 and 5.4 Å for [bmim] and [bmmim], respectively. This suggests that interactions with CO_2 are dominated by the anion. Figure 8 also shows that the CO_2−anion interactions are mostly independent of the cation; the location and shape of the initial $g(r)$ peak are the same for both liquids. In other words, the simulations indicate that CO_2 strongly associates with the $[PF_6]$ anion, regardless of the nature of the cation. These results, together with the experimental findings described earlier, demonstrate that it is the anion that governs the overall solubility of CO_2 in imidazolium-based ionic liquids, with the nature of the cation playing a secondary role. The way in which CO_2 associates with the anion can be seen by examining Figure 9, which shows $g(r)$ and $I(r)$ for a single CO_2 oxygen atom and the anion phosphorus (a) and fluorine (b) atoms. Consistent with Figure 8, the CO_2 oxygen atoms are closer to the anion than to the C2 carbon of the cation. There is a single initial peak on the O−P $g(r)$ but a split initial peak for the O−F $g(r)$. This is due to the fact that the linear CO_2 molecule aligns in such a way so as to be "tangent" to the spherical anion while maximizing favorable interactions. The plots are essentially identical for the two liquids, again confirm-

a)

b)
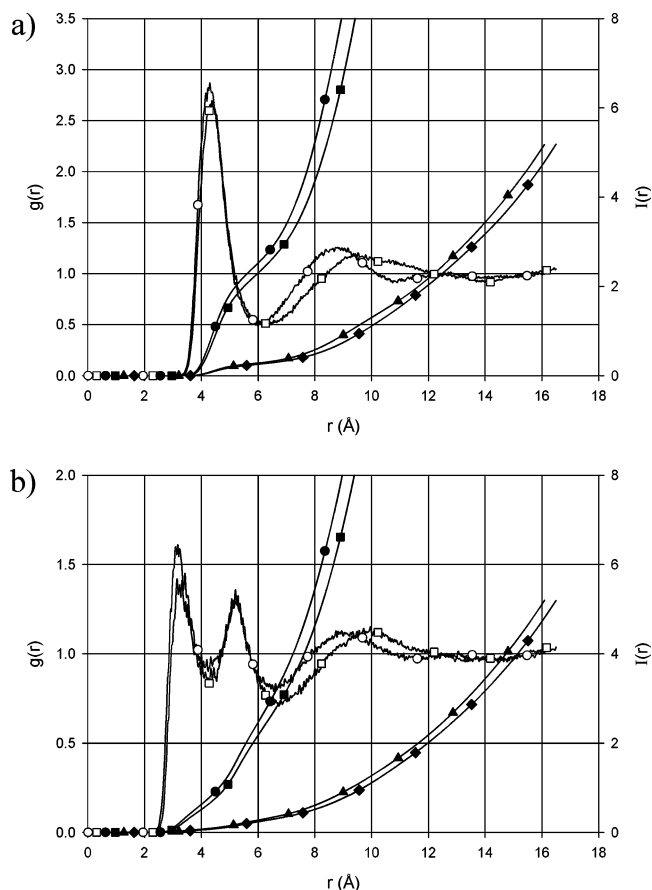
Figure 9. (a) Radial distribution functions and number integrals for the oxygen atoms of CO_2 and the phosphorus atom of $[PF_6]$. (b) Same plot as (a), but for the oxygen atoms of CO_2 about the fluorine atoms of $[PF_6]$. Symbol meanings: $g(r)$ for [bmim], ○; $g(r)$ for [bmmim], □; $I(r)$ for [bmim]-$[PF_6]$ phosphorus (a) or fluorine (b) atom about the CO_2 oxygen, ●; $I(r)$ for $[bmmim][PF_6]$ phosphorus (a) or fluorine (b) atom about the CO_2 oxygen, ■; $I(r)$ for the CO_2 oxygen about the phosphorus (a) or fluorine (b) of $[bmim][PF_6]$, ▲; $I(r)$ for the CO_2 oxygen about the phosphorus (a) or fluorine (b) atom of $[bmmim][PF_6]$, ◆.

ing that the dominant CO_2−anion interactions are not much affected by the subtle differences in cation structure.

6. Conclusions

Experimental and molecular simulation studies focused on understanding the factors governing the high solubility of CO_2 in alkylimidazolium-based ionic liquids have been carried out. In agreement with previous spectroscopic studies,[14,15] it is found that the anion dominates the interactions with the CO_2, with the cation playing a secondary role. Simulations indicate that CO_2 organizes strongly about the $[PF_6]$ anion in a "tangent-like" configuration that maximizes favorable interactions, but is more diffusely distributed about the imidazolium ring. We expect that the $[BF_4]$ and $[Tf_2N]$ anions also have strong association with CO_2. Replacing the acidic hydrogen on the C2 carbon of the [bmim] cation with a methyl group leads to a reduction in the experimental enthalpy of absorption by about 1−3 kJ/mol and a modest loss of organization of the anion and CO_2 about the cation. The major factor controlling CO_2 solubility in this class of ionic liquids is the nature of the anion. The results suggest that the association of CO_2 with the anion is the best indicator of CO_2 solubility in alkylimidazolium-based ILs. Changes in the imidazolium cation involving alkyl groups are expected to have relatively little influence on CO_2 solubility.

Both the simulations and the experiments indicate that the molar density of ionic liquids increases significantly with the addition of 10 mol % CO_2, because there is almost no volume expansion when the CO_2 is added. This is in contrast to conventional solvents that show a very small molar density increase because the solvent expands when CO_2 is added. Consistent with this finding, the cation–anion radial distribution functions change very little upon addition of CO_2 into the system. That is, the underlying fluid structure of the IL is relatively unperturbed by the addition of CO_2, due to the strong Coulombic interactions responsible for the organization of the liquid.

Supporting Information Available: A complete listing of all force field parameters used in this work (PDF). This material is available free of charge via the Internet at http://pubs.acs.org.

JA039615X